ADVANCED FUNCTIONAL MATERIALS
www.afm-journal.de



# Rational Design of a Printable, Highly Conductive Silicone-based Electrically Conductive Adhesive for Stretchable Radio-Frequency Antennas

*Zhuo Li, Taoran Le, Zhenkun Wu, Yagang Yao, Liyi Li, Manos Tentzeris, Kyoung-Sik Moon,* and C. P. Wong**

**Stretchable radio-frequency electronics are gaining popularity as a result of the increased functionality they gain through their flexible nature, impossible within the confines of rigid and planar substrates. One approach to fabricating stretchable antennas is to embed stretchable or flowable conductive materials, such as conductive polymers, conductive polymer composites, and liquid metal alloys as stretchable conduction lines. However, these conductive materials face many challenges, such as low electrical conductivity under mechanical deformation and delamination from substrates. In the present study, a silicone-based electrically conductive adhesive (silo-ECA) is developed that have a conductivity of $1.51 \times 10^4$ S cm$^{-1}$ and can maintain conductivity above $1.11 \times 10^3$ S cm$^{-1}$, even at a large stain of 240%. By using the stretchable silo-ECAs as a conductor pattern and pure silicone elastomers as a base substrate, stretchable antennas can be fabricated by stencil printing or soft-lithography. The resulting antenna's resonant frequency is tunable over a wide range by mechanical modulation. This fabrication method is low-cost, can support large-scale production, has high reliability over a wide temperature range, and eliminates the concerns of leaking or delamination between conductor and substrate experienced in previously reported micro-fluidic antennas.**

## 1. Introduction

Research and development in modern electronics strives for increased functionality and reduced form factor. Stretchable radio-frequency (RF) electronics are gaining popularity as a result of the enhanced functionality they gain through their flexible nature, impossible within the confines of rigid and planar substrates. Stretchable RF electronics not only enable applications in which circuits can be wrapped conformally around complex curvilinear shapes or biological tissues, such as in body-worn wireless sensor nodes,[1,2] and wearable radio frequency identification (RFID) tags,[3] but also allow facile tuning of the resonant frequency by mechanical deformation.[4,5] However, the field of stretchable RF electronics is still in its infancy, and like other emerging electronic technologies, new materials and processing methods are the two driving forces for their ever-improving development and performance.

There are currently two general approaches to the fabrication of stretchable electronics. The first utilizes conventional rigid materials, but employs elegantly designed wavy or arc-shaped structures that are capable of accommodating applied strains of 100% or more.[2,6,7] The second approach is to maintain the conventional circuit layout, but embed stretchable or flowable conductive materials, such as conductive polymers,[8,9] conductive polymer composites,[10] and liquid metal alloys[4,11] as stretchable conduction lines. For antennas, this second approach is usually preferred because of its relative simplicity in circuit design and fabrication. However, this approach imposes stringent requirements for the conductive materials, including 1) high electrical conductivity to achieve high-efficiency for the RF devices;[9] and 2) high elasticity to provide a tunable resonant frequency,[4] and 3) maintaining a similar electrical conductivity under applied strain. Conductive polymers and carbon-based conductive composites have conductivities at least three orders of magnitude lower than those of metals, leading to an inferior electrical efficiency values;[9] and liquid metal alloys usually present the fundamental problems of a high freezing temperature (limiting their usage in cold weather), thermal expansion coefficient mismatch with dielectric substrates, and a tendency towards leakage.[4]

Here we report the use of stretchable silicone-based electrically conductive adhesives (silo-ECAs) as conductor and pure silicone elastomers as substrate for the fabrication of stretchable antennas. Silicone rubbers feature a unique combination of high elasticity, biocompatibility,[12] patternability,[13] and low

Z. Li, Z. Wu, Y. Yao, L. Li, Dr. K.-S. Moon, Prof. C. P. Wong
School of Materials Science and Engineering
Georgia Institute of Technology
Atlanta, GA 30332, USA
E-mail: ks.moon@mse.gatech.edu; cp.wong@mse.gatech.edu
T. Le, Prof. M. Tentzeris
School of Electrical and Computer Engineering
Georgia Institute of Technology
Atlanta, GA 30332, USA
Prof. C. P. Wong
Department of electronic Engineering
The Chinese University of Hong Kong
Sha Tin, Hong Kong

DOI: 10.1002/adfm.201403275


© 2014 WILEY-VCH Verlag GmbH & Co. KGaA, Weinheim

dielectric constant and low dissipation, making them an excellent candidate for stretchable antenna substrates. The silicone substrate selected in the present study, Elastosil M 4642, has an elongation at break of 787%, suitable patternability by soft-lithography, and a low dielectric constant ca. 3 and a dissipation factor <0.01 for 10 MHz–1 GHz (Figure S1, Supporting Information). More importantly, the conductor material for building the antenna, the silo-ECA is rationally designed to achieve 1) a high conductivity at both static ("zero stretch") and stretched states guaranteeing a high radiation efficiency for both configurations; 2) a proper viscosity to enable stencil printing or soft-lithography for high-resolution and large scale fabrication; and 3) cross-linking with the silicone substrate to eliminate delamination and leaking issues. As a proof of concept, we use these materials to fabricate a quarter-wavelength bow-tie antenna that can be tuned from 3.45 GHz to 2.42 GHz by simple mechanical stretching to 60% strain, while maintaining a very low reflected power level below –15 dB.

## 2. Results and Discussion

### 2.1. Enhancement of Electrical Conductivity of silo-ECAs

High conductivity is one of the most critical requirements for the silo-ECAs to be used in stretchable antennas, because it will affect the conduction loss and thus the radiation efficiency. Conventional antennas are usually built with copper, which has a conductivity of $5.96 \times 10^5$ S cm$^{-1}$.[14] Elastomers filled with conductive polymers or carbon materials can be easily stretched but their conductivity is at least three orders of magnitudes lower than that of copper,[15–21] inevitably resulting in a reduced radiation efficiency.[9] Therefore, silver-filled silo-ECAs are used as the conductor in this study. ECAs have gained increasing popularity as an environmentally friendly alternative to Sn/Pb solders.[22] Conventional ECAs are mostly using epoxy as polymer matrix since the curing shrinkage of epoxy can pack the silver fillers tightly and develop a high conductivity.[23] The curing shrinkage of silicone is much weaker than that of epoxy; hence the conductivity needs to be improved through surface modification of the silver fillers in silo-ECAs. The first modification is using long-chain hydride-terminated polydimenthyl siloxane (H-PDMS) as the curing agent of the silo-ECA matrix and a reducing agent simultaneously. Commercial silver flakes are usually covered with a thin layer of lubricant, whose component is generally a long chain fatty acid. The existence of this lubricant on the silver surface is demonstrated by Raman spectra and thermogravimetric analysis (TGA) in Figure S2 (Supporting Information). The carboxylic group of the fatty acid can coordinate with the silver surface and form a silver carboxylate salt complex, while the hydrocarbon chain can facilitate the dispersion of silver flakes and prevent oxidation.[24] However, these lubricants are electrically insulating by nature, posing a significant energy barrier to electron conduction between neighboring silver flakes. It has been found that a reducing agent added in ECAs chemically reduces the coordinated silver salt to nano/submicrometer-sized silver particles and these in situ formed nano/submicrometer-sized particles may then facilitate the sintering of the silver flakes during curing.[25,26] H-PDMS, which is a typical curing agent for vinyl-modified siloxane prepolymers, has also been demonstrated to have such a reducing capability.[27,28] To support this, H-PDMS was reacted with silver stearate at 160 °C and the generated silver nanoparticles were clearly detected by UV/Visible spectra, X-ray diffraction (XRD) and transmission electron microscopic (TEM) (Figure S3, Supporting Information). As a result, the high molecular weight H-PDMS is used in the formulation not only to provide a high elasticity due to the low cross-linking density of the formed silicone matrix (Figure S4, Supporting Information), but also to enhance the electrical conductivity via the generation and sintering of silver nanoparticles.[28] The second modification made to the filler particles is the iodination of the silver flakes before mixing with the silicone matrix. It was found that nonstoichiometric Ag/AgI nanoislands sparsely formed on the silver flake surface by iodination treatment could activate the silver surfaces by exposing fresh silver from inside flakes to the surface.[29] The exposure of fresh silver at the flake surface further facilitates the sintering between silver flakes during curing.

The combination of these two surface modification methods can form a strong electron conduction network and reach an initial conductivity of $1.51 \times 10^4$ S cm$^{-1}$ filled with 80 wt% silver flakes, which is comparable with that of conventional epoxy-based ECAs and in the same order of magnitude with those of many metals.[25,30]

### 2.2. Maintaining the High Conductivity During Stretching

For stretchable electronics applications, maintaining a high conductivity of silo-ECA during stretching is as important as obtaining the high initial conductivity. Polymer composites loaded with conductive fillers usually experience significant conductivity change under mechanical strain. This response, called the piezoresistive effect, results from the displacement of fillers within the matrix. Analytical models of the piezoresistance of polymer composites filled with carbon black,[31] CNTs,[32] and metal spheres[33] have been extensively studied and the conductivity after stretching is given by

$$\sigma_1 \approx \sigma_0 \exp\left[\frac{4\pi\sqrt{2m\varphi}}{h}(s_0 - s_1)\right] \quad (1)$$

where, $\sigma_0$ and $\sigma_1$ are the conductivity before and after stretching, $h$ is Plank's constant, $\varphi$ is the height of the tunneling potential barrier, $m$ is the mass of an electron, and $s_0$ and $s_1$ are the average interparticle distance between fillers before and after stretching, respectively. According to this equation, in order to maintain the conductivity after mechanical deformation, one can either reduce the tunneling potential barrier $\varphi$ or minimize the interparticle distance $s_1$ during stretching. The surface modification methods mentioned above remove the insulating lubricant on the silver flake surfaces and thus reduce the tunneling potential barrier $\varphi$ between the silver flakes, which not only benefit the initial conductivity but also mitigate the conductivity change upon stretching.

In order to minimize the interparticle distance $s_1$, the shape and morphology of the silver fillers used in silo-ECA are carefully


© 2014 WILEY-VCH Verlag GmbH & Co. KGaA, Weinheim

engineered and fillers with a high aspect ratio are desired. Previous studies have mostly focused on 1-D high aspect ratio fillers, such as CNTs and silver nanowires.[7,15,16,18,19,21,34,35] However, in the case of aligned fillers, such as ultra-long SWNTs,[15,16] the conductivity is maintained only if the applied stress is in the longitudinal direction of the fillers, whereas extension in other directions causes poor conductivity. In the case of the randomly dispersed 1-D fillers, though they begin with a random network, they will become aligned under the applied stress during stretching. The contacts will be maintained in the stretching direction, but the loss of the number of conduction paths in the other two directions may decrease the overall conductivity of the composite.[36] Therefore, 2-D silver flakes are selected as fillers in this study. Silver flakes are stacked parallel to each other by the shear force in printing processes.[37] As a result, even after stretching the stacking allows silver flakes to keep the tunneling distance almost unaltered within a certain strain range, because the sliding between parallel flakes in the X-Y direction does not alter the distance between these flakes (**Figure 1**a). As such, the resistance can be kept similar at a certain range of tensile strain. In addition to the shape design, secondary textures due to the in situ formation of silver nanoparticles from chemical reduction of the silver carboxylate complex (lubricant) are another important factor in reducing the interparticle distance. As illustrated in Figure 1b, these secondary textures could reduce the tunneling distance without changing the filler loading. This texture not only enhances the electrical conductivity of ECAs in the static state but also mitigates the interparticle separation in the stretched state.

For the conductivity measurement during stretching, a strip of silo-ECA is printed on silicone substrate and cut into a dumbbell shape, as shown in Figure S5 (Supporting Information). The specimen is then mounted on a tensile tester (Instron Microtester 5548). Real-time electrical resistance change is measured by a typical four-wire method with all the wires "soldered" to the silo-ECA stripe with additional silo-ECA and the applied strain is simultaneously recorded by the tensile tester. The conductivity of the silo-ECA drops to $5.03 \times 10^3$ S cm$^{-1}$ after embedding in the substrate, yet it is still higher than most previously reported stretchable conductors. Figure 1c shows the conductivity change as a function of the applied tensile strain of the silo-ECA as compared with previously reported stretchable conductors. A general trend is visible; the metal-filled conductive composites[34,38,39] have significantly higher conductivity than carbon-filled conductive composites,[15–19] while some CNT-based composites can maintain a high conductivity at a larger elongation due to their high-aspect ratio.[18] The conductivity of the silo-ECA is two orders of magnitude higher than that of conventional silver/PDMS composites[38] due to the surface treatments mentioned above, and is comparable with gold nanoparticle/polyurethane composites.[39] More importantly, silo-ECA has better elasticity than previously reported metal/polymer composites and can maintain a high conductivity at large deformations. For example, even at a strain of 240%, the conductivity is still as high as $1.11 \times 10^3$ S cm$^{-1}$, indicating that the external stress only leads to sliding between overlapping flakes and does not change the tunneling distance significantly. In addition, the conductivity change is within 25%

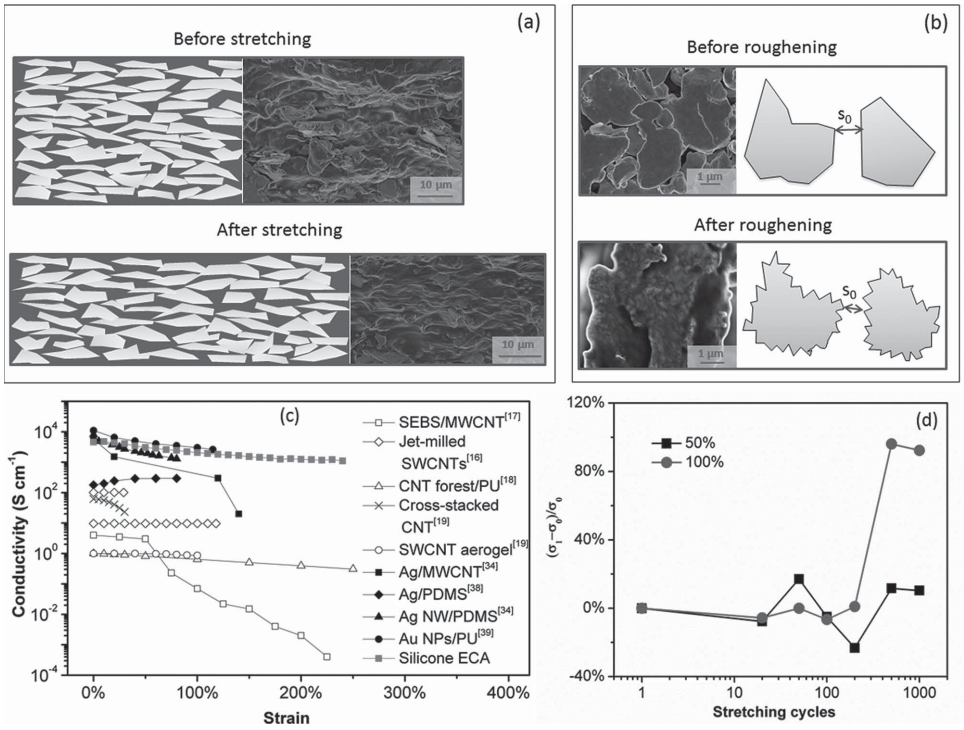


**Figure 1.** a) Schematic illustration and SEM images of the silver flakes before and after stretching. The displacement is mostly in the *X–Y* direction. b) SEM images and schematic illustration showing the roughening process of the silver flakes by H-PDMS can decrease the interparticle distance between neighboring flakes. c) Conductivity change of the silo-ECA as a functional of tensile strain, as compared with the values from previous studies. d) The conductivity of silo-ECA after cycling at 50% strain and 100% strain.


© 2014 WILEY-VCH Verlag GmbH & Co. KGaA, Weinheim

after 1000 cycles of stretching at 50% applied strain (Figure 1d). When we increase the tensile strain to 100%, the conductivity remains almost invariant over the first 500 cycles, and then even increases to double its previous value. The increase in conductivity may result from the further alignment of flakes in X,Y-direction by the mechanical stretching, giving rise to a better conductivity in the *X,Y*-direction. Maintaining the low resistance at a very large strain is essential to have an impedance match for the antenna in the stretching state. Apparently, with a relatively slight change of conductivity at large strains, these silo-ECAs are highly suitable for building stretchable antennas.

### 2.3. Fabrication of Stretchable Antennas

Another advantage of the hereby-presented silo-ECA is the printability of the material in fine patterns, which is critical for the fabrication of stretchable antennas. In liquid-metal-based antennas, the antenna pattern is formed by injecting liquid metal into a pre-patterned PDMS substrate with micro-fluid channels.[4] This method is difficult to fabricate complex patterns and presents various leakage concerns. A CNT-based antenna is made by printing CNT paste on PDMS substrate, but the weak adhesion of the CNT paste to PDMS substrate may limit the resolution of the printed patterns.[16] With a suitable viscosity of ca.161 Pa.s at room temperature and a chemical bonding to the silicone substrate during curing, the silo-ECA is capable of high-definition stencil-printing as well as soft lithography to fabricate stretchable antennas. **Figure 2**a,b illustrates the two processes to fabricate the antenna pattern. In the stencil printing process, ECA is stencil-printed on a PTFE board and is partially cured. Then the ECA pattern is covered by pure silicone. After curing the ECA and silicone, the bonded silicone substrate and ECA are both peeled off from the PTFE board and form the stretchable antenna. It should be noted that during the curing process, cross-linking occurs at the interface between ECA and silicone substrate, eliminating the delamination issues. In the soft-lithography process, a master mold is fabricated by patterning a silicon wafer via photolithography. Then the silicon wafer is treated with 1*H*,1*H*,2*H*,2*H*-perfluorododecyltrichlorosilane to make it hydrophobic and to facilitate the peeling of the silicone substrate from the silicon wafer. A silicone pre-polymer is poured onto the master mold and is cured to form an elastomeric mold. After peeling off the silicone elastomeric mold, the silo-ECA is dispensed into the cavity of the silicone substrate to form the conductive pattern before getting cured. Figure 2c-f show the printed lines and circles created by the two methods. Patterns on the scale of hundreds of micrometers can be accurately replicated through both methods, though the soft-lithography process can duplicate shapes with clearer definition and more uniform thickness.

### 2.4. Antenna Performance

High conductivity and elasticity, as well as easy fabrication, make our silo-ECA a promising building block for stretchable RF devices. For proof-of-concept demonstration purposes, one half-wavelength bow-tie antenna (**Figure 3**a) and one quarter-wavelength bow-tie antenna (Figure 3b) are fabricated through the soft-lithography process (Figure 3c,d). It is clear that the fabricated antenna samples correspond well to the original design dimensions.

The reflected electromagnetic (EM) power performance of these two antennas is characterized with a vector network analyzer (VNA) and compared with the simulated data. If the antenna radiates efficiently at certain frequency, the majority of incident EM power is radiated into space with little reflected power. For the half-wavelength antenna shown in Figure 3e, the measured resonant frequency is located at 1.75 GHz for an operation range of 50 MHz–3 GHz, slightly lower than the simulated value of 1.85 GHz. The return loss, also known as $|S_{11}|$, is –18.5 dB, which is lower than the simulated value of –13.1 dB, indicating that more than 99% power has been transmitted at this frequency. The bandwidth of the actual antenna is larger than that of the simulated data, leading to a lower Q factor. This lowered Q factor should result from the conduction loss of the ECA material. For the quarter-wavelength antenna (Figure 3f), the measured resonant frequency lies in 3.50 GHz at the range of 50 MHz–4 GHz, very close to the simulated value of 3.45 GHz.

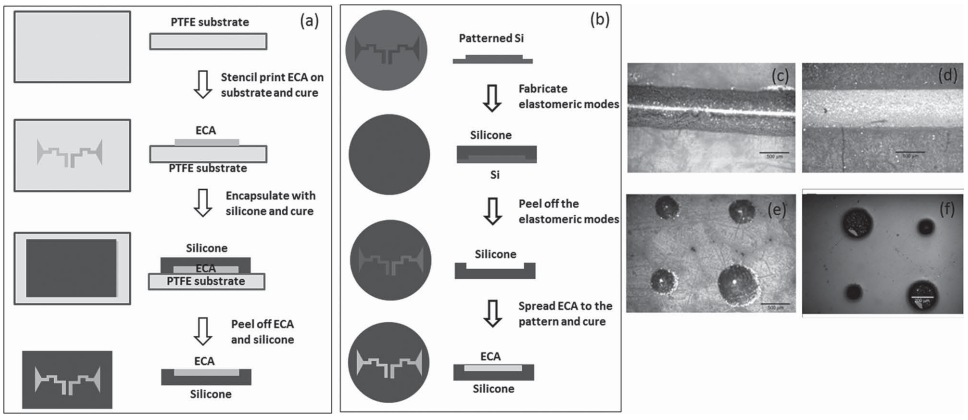


**Figure 2.** a) Stencil printing process to fabricate a stretchable antenna. b) Soft-lithography process to fabricate a stretchable antenna. Lines printed by c) stencil printing and d) soft-lithography. Circles printed by e) stencil printing and f) soft-lithography.


© 2014 WILEY-VCH Verlag GmbH & Co. KGaA, Weinheim

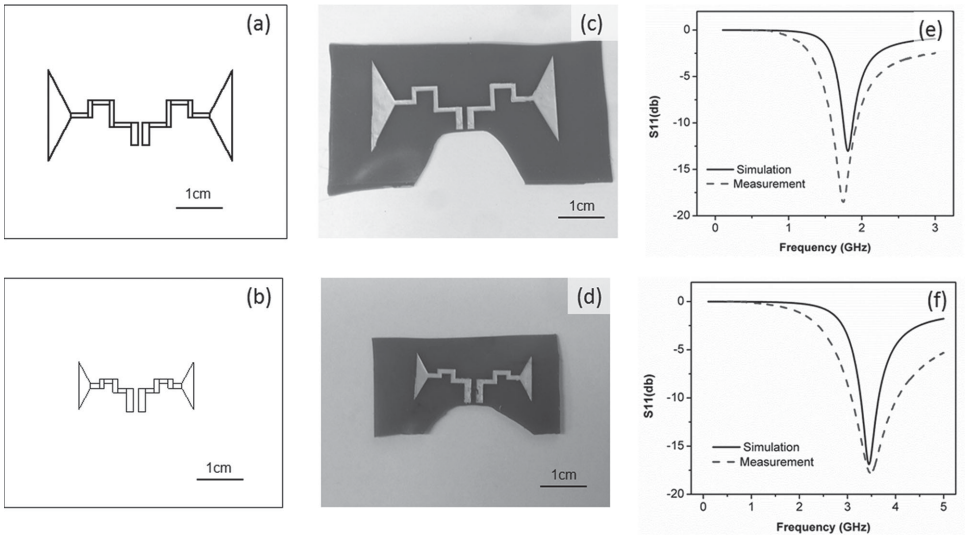


**Figure 3.** a,b) The design of bow-tie antenna with two different sizes; c,d) Bow-tie antenna fabricated by soft-lithography process; e,f) The measured and simulated reflected EM power as a function of frequency. The upper row shows the results of half-wavelength antenna and the lower row shows the results of quarter-wavelength antenna.

The $|S_{11}|$ of the fabricated antenna prototype is –17.7 dB, also slightly lower than the simulated value of –16.9 dB, which indicates that the fabricated antenna is better matched with 50 Ω input at this certain frequency. Similar to the half-wavelength antenna, the actual bandwidth of the fabricated quarter-wavelength antenna is larger than that of the simulated result.

**Figure 4** illustrates the performance of the quarter-wavelength antenna under different tensile strains. The dimension change of the antenna is simulated by finite element analysis and then loaded into the high frequency structural simulator (HFSS) to predict the return loss of the deformed antenna. In order to determine the actual antenna performance under strain, the prepared quarter-wavelength antenna is mounted on the tensile tester and its return loss is measured by the VNA during stretching. As shown in Figure 4a, the resonant frequency decreases monotonically from 3.45 to 2.42GHz as it is stretched to 60% strain, demonstrating the tunability of the fabricated antenna over a wide range of frequency by simple mechanical modulation. The consistent agreement between measurement and simulation suggests the frequency tuning can be predicted theoretically. Figure 4b shows that the return loss of the antenna is kept below –15 dB when the antenna is stretched by up to 60%, indicating that the high-quality radiation efficiency is maintained throughout different stretching conditions. After retracting, the resonant frequency returns to 3.45 GHz. It should be noted that the antenna could be stretched to strains larger than 60%, but the connections with the SMA connector become weak and may cause mismatching.

## 3. Conclusions

In conclusion, we have developed silo-ECA materials that have a conductivity of $1.51 \times 10^4$ S cm$^{-1}$ and can maintain conductivity above $1.11 \times 10^3$ S cm$^{-1}$, even at a large stain of 240%. By using the stretchable silo-ECAs as a conductor pattern and pure silicone elastomers as a base substrate, stretchable antennas can be fabricated by stencil printing or

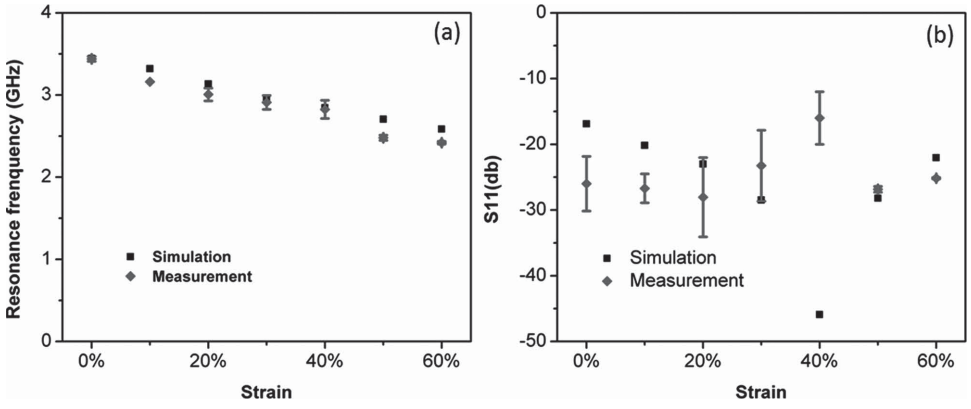


**Figure 4.** a) The simulated and measured resonant frequency of the quarter-wavelength antenna as a function of tensile strain; b) The simulated and measured return loss of the quarter-wavelength antenna as a function of tensile strain.


© 2014 WILEY-VCH Verlag GmbH & Co. KGaA, Weinheim

soft-lithography. The resulting antenna's resonant frequency is tunable over a wide range by mechanical modulation. This fabrication method is low-cost, can support large-scale production, has high reliability over a wide temperature range, and eliminates the concerns of leaking or delamination between conductor and substrate experienced in previously reported micro-fluidic antennas.

## 4. Experimental Section

*Synthesis of Silo-ECA*: The silicone matrix for the silo-ECAs is prepared by mixing vinyl-modified PDMS (Wacker V1K) and hydride-terminated PDMS (Gelest H41) with a molar ratio of 1:1. Platinum(0)-1,3-divinyl-1,1,3,3-tetramethyldisiloxane complex (50 ppm, Sigma-Aldrich Co.) was used as catalyst. The iodination treatment of silver flakes was performed by dispersing the flakes (Silflake 144) in an ethanol solution of iodine (0.5 μmol $L^{-1}$) for 1 h. Then a simple filtration was performed to wash out remaining iodine, and the flakes were dried in a vacuum oven for 24 h.[29] In a typical ECA formulation, iodine treated silver flake (80 wt%) and the above silicone mixture (20 wt%) were homogenized for 5 min. Curing was carried out at 160 °C for 1 h.

*Characterization*: The mechanical properties of the silicone substrate were tested in a typical tensile test setup (Instron microtester 5548). Specimens were cut into a dumbbell shape (Figure S1a, Supporting Information) and tested at a rate of 10 mm/min. The dielectric properties were measured by an RF impedance analyzer (Agilent E4991A). To measure the electrical conductivity, the paste was cast in a Teflon mold (22 mm × 7 mm × 0.5 mm). After curing at 160 °C for 1 h, the bulk resistance of the film was measured by the four-wire method with a Keithley 2000 multimeter. The thickness was measured by a profilometer (Heidenhain ND 281, Germany). Electrical conductivity $\sigma$ was then calculated by

$$\sigma = \frac{l}{Rwt}$$

where $R$ is the bulk resistance and $l$, $w$, and $t$ are the length, width, and thickness of the film, respectively. Raman spectra of silver flakes were obtained by a LabRAM ARAMIS Raman confocal microscope (HORIBA Jobin Yvon) equipped with a 532 nm diode pumped solid state (DPSS) laser. Si wafer was used as a substrate. The decomposition of the lubricants on the surface of silver flakes was studied by TGA (TA Instruments, Q50) with a heating rate of 5 °C $min^{-1}$ in nitrogen. H-PDMS treated silver flakes are prepared by immersing silver flakes in H-PDMS at 160 °C for 30 min. The treated silver flakes are washed with toluene in three centrifuge cycles in order to remove the remaining H-PDMS and with acetone in another three cycles to remove the products of the surfactant reduction reaction. Then the silver flakes are dried in vacuum before morphology observation by a field emission scanning electron microscope (FE-SEM, LEO 1530). The nanoparticles generated by reacting silver stearate and hydride-terminated PDMS were dispersed in toluene and dried in a copper grid before being characterized by TEM (JEOL 100CX). The nanoparticle colloidal in toluene was also characterized by UV–VIS spectroscopy (Shimadzu UV-2450). Powder XRD analysis was carried out with a Philips X-pert alpha-1 diffractometer, using Cu $K_\alpha$ radiation (45 KV and 40 mA). The complex viscosity of uncured silo-ECA was measured using a discovery hybrid rheometer (TA Instruments, HR2). The dimension change of the fabricated quarter-wavelength antenna during stretching was simulated using COMSOL multiphysics. A rectangular substrate (35 mm × 30 mm × 0.7 mm) was stretched in the simulation, with the assumption that silicone substrate has a Poisson's ratio of 0.49.[40] The simulation of antenna performance was conducted by HFSS from Agilent. The S11 parameter was measured with a VNA (Rohde-Schwarz, R&S ZVA 8).

## Supporting Information

Supporting Information is available from the Wiley Online Library or from the author.

## Acknowledgements

The authors acknowledge Technic Inc. and Wacker Chemie AG for donating the silver flakes and silicone resin, respectively. The authors are also grateful for the useful discussion with Dr. Daniela Staiculescu, Mr. Josh Agar, and Ms. Fan Cai.

Received: September 19, 2014
Revised: October 23, 2014
Published online: November 25, 2014

[1] L. Gatzoulis, I. Iakovidis, *IEEE Eng. Med. Biol. Mag.* **2007**, *26*, 51.
[2] S.-W. Hwang, X. Huang, J.-H. Seo, J.-K. Song, S. Kim, S. Hage-Ali, H.-J. Chung, H. Tao, F. G. Omenetto, Z. Ma, J. A. Rogers, *Adv. Mater.* **2013**, *25*, 3526.
[3] D.-H. Kim, J. Viventi, J. J. Amsden, J. Xiao, L. Vigeland, Y.-S. Kim, J. A. Blanco, B. Panilaitis, E. S. Frechette, D. Contreras, D. L. Kaplan, F. G. Omenetto, Y. Huang, K.-C. Hwang, M. R. Zakin, B. Litt, J. A. Rogers, *Nat. Mater.* **2010**, *9*, 511.
[4] M. Kubo, X. Li, C. Kim, M. Hashimoto, B. J. Wiley, D. Ham, G. M. Whitesides, *Adv. Mater.* **2010**, *22*, 2749.
[5] L. Song, A. C. Myers, J. J. Adams, Y. Zhu, *ACS Appl. Mater. Interfaces* **2014**, *6*, 4248.
[6] a) X. Hu, P. Krull, B. de Graff, K. Dowling, J. A. Rogers, W. J. Arora, *Adv. Mater.* **2011**, *23*, 2933; b) D.-H. Kim, J. A. Rogers, *Adv. Mater.* **2008**, *20*, 4887; c) J. Lee, J. Wu, M. Shi, J. Yoon, S.-I. Park, M. Li, Z. Liu, Y. Huang, J. A. Rogers, *Adv. Mater.* **2011**, *23*, 986; d) T. Li, Z. Huang, Z. Suo, S. P. Lacour, S. Wagner, *Appl. Phys. Lett.* **2004**, *85*, 3435; e) S. P. Lacour, J. Jones, S. Wagner, T. Li, Z. Suo, *Proc. IEEE* **2005**, *93*, 1459; f) S. P. Lacour, S. Wagner, Z. Huang, Z. Suo, *Appl. Phys. Lett.* **2003**, *82*, 2404; g) Y. Zhang, H. Fu, Y. Su, S. Xu, H. Cheng, J. A. Fan, K.-C. Hwang, J. A. Rogers, Y. Huang, *Acta Mater.* **2013**, *61*, 7816; h) X. Huang, H. Cheng, K. Chen, Y. Zhang, Y. Zhang, Y. Liu, C. Zhu, S.-c. Ouyang, G.-W. Kong, C. Yu, Y. Huang, J. A. Rogers, *IEEE Trans. Biomed. Eng.* **2013**, *60*, 2848; i) Y. Zhang, S. Wang, X. Li, J. A. Fan, S. Xu, Y. M. Song, K.-J. Choi, W.-H. Yeo, W. Lee, S. N. Nazaar, B. Lu, L. Yin, K.-C. Hwang, J. A. Rogers, Y. Huang, *Adv. Funct. Mater.* **2014**, *24*, 2028; j) J. A. Fan, W. H. Yeo, Y. Su, Y. Hattori, W. Lee, S. Y. Jung, Y. Zhang, Z. Liu, H. Cheng, L. Falgout, M. Bajema, T. Coleman, D. Gregoire, R. J. Larsen, Y. Huang, J. A. Rogers, *Nat. Commun.* **2014**, *5*, 3266; k) S. Xu, Y. Zhang, L. Jia, K. E. Mathewson, K.-I. Jang, J. Kim, H. Fu, X. Huang, P. Chava, R. Wang, S. Bhole, L. Wang, Y. J. Na, Y. Guan, M. Flavin, Z. Han, Y. Huang, J. A. Rogers, *Science* **2014**, *344*, 70.
[7] Y. Sun, W. M. Choi, H. Jiang, Y. Y. Huang, J. A. Rogers, *Nat. Nano.* **2006**, *1*, 201.
[8] A. Verma, W. Bo, R. Shepherd, C. Fumeaux, T. Van-Tan, G. G. Wallace, B. D. Bates, "6 GHz microstrip patch antennas with PEDOT and polypyrrole conducting polymers", presented at *2010 Int. Conf. Electromagnetics in Advanced Applications (ICEAA)*, 20–24 Sept. 2010, **2010**.
[9] T. Kaufmann, A. Verma, V.-T. Truong, B. Weng, R. Shepherd, C. Fumeaux, *Int. J. Antenn. Propag.* **2012**, *2012*, 11.
[10] a) J. Agar, J. Durden, D. Staiculescu, R. Zhang, E. Gebara, C. P. Wong, "Electrically conductive silicone nano-composites for stretchable RF devices", presented at *Microwave Symposium*


© 2014 WILEY-VCH Verlag GmbH & Co. KGaA, Weinheim

*Digest (MTT), 2011 IEEE MTT-S International* 5–10 June 2011, 2011; b) J. C. Agar, K. J. Lin, R. Zhang, J. Durden, K.-S. Moon, C. P. Wong, "Novel PDMS(silicone)-in-PDMS(silicone) : Low cost flexible electronics without metallization", presented at *The 60th Electronic Components and Technology Conference, IEEE* 1–4 June 2010, 2010; c) Y. Bayram, Y. J. Zhou, B. S. Shim, S. M. Xu, J. A. Zhu, N. A. Kotov, J. L. Volakis, *IEEE Trans. Antennas Propagat.* **2010**, *58*, 2732.

[11] a) M. D. Dickey, R. C. Chiechi, R. J. Larsen, E. A. Weiss, D. A. Weitz, G. M. Whitesides, *Adv. Funct. Mater.* **2008**, *18*, 1097; b) C. Shi, A. Rydberg, K. Hjort, W. Zhigang, *Appl. Phys. Lett.* **2009**, *94*, 144103; c) J.-H. So, J. Thelen, A. Qusba, G. J. Hayes, G. Lazzi, M. D. Dickey, *Adv. Funct. Mater.* **2009**, *19*, 3632.

[12] J. C. McDonald, G. M. Whitesides, *Acc. Chem. Res.* **2002**, *35*, 491.

[13] a) H. Cong, T. Pan, *Adv Funct Mater* **2008**, *18*, 1912; b) D. Cai, A. Neyer, *Microfluid Nanofluid* **2010**, *9*, 855.

[14] D. C. Giancoli, *Physics for Scientists and Engineers with Modern Physics*, Pearson Education Inc., Upper Saddle River, New Jersey **2008**.

[15] T. Sekitani, Y. Noguchi, K. Hata, T. Fukushima, T. Aida, T. Someya, *Science* **2008**, *321*, 1468.

[16] T. Sekitani, H. Nakajima, H. Maeda, T. Fukushima, T. Aida, K. Hata, T. Someya, *Nat. Mater.* **2009**, *8*, 494.

[17] Y. Li, H. Shimizu, *Macromolecules* **2009**, *42*, 2587.

[18] M. K. Shin, J. Oh, M. Lima, M. E. Kozlov, S. J. Kim, R. H. Baughman, *Adv. Mater.* **2010**, *22*, 2663.

[19] a) K. Liu, Y. Sun, P. Liu, X. Lin, S. Fan, K. Jiang, *Adv. Funct. Mater.* **2011**, *21*, 2721; b) K. H. Kim, M. Vural, M. F. Islam, *Adv. Mater.* **2011**, *23*, 2865.

[20] a) T. S. Hansen, K. West, O. Hassager, N. B. Larsen, *Adv. Funct. Mater.* **2007**, *17*, 3069; b) M. Vosgueritchian, D. J. Lipomi, Z. Bao, *Adv. Funct. Mater.* **2012**, *22*, 421.

[21] a) F. Xu, X. Wang, Y. Zhu, Y. Zhu, *Adv. Funct. Mater.* **2012**, *22*, 1279; b) Y. Zhang, C. J. Sheehan, J. Zhai, G. Zou, H. Luo, J. Xiong, Y. T. Zhu, Q. X. Jia, *Adv. Mater.* **2010**, *22*, 3027.

[22] Y. Li, K.-s. Moon, C. P. Wong, *Science* **2005**, *308*, 1419.

[23] D. Lu, Q. K. Tong, C. P. Wong, *IEEE Trans. Compon. Packag. Technol.* **1999**, *22*, 223.

[24] a) D. Lu, Q. K. Tong, C. P. Wong, *IEEE Trans. Compon. Packag. Technol.* **1999**, *22*, 365; b) D. Lu, C. Wong, *J. Therm. Anal. Calorim.* **2000**, *59*, 729; c) D. Lu, C. Wong, *J. Therm. Anal. Calorim.* **2000**, *61*, 3.

[25] R. Zhang, K.-s. Moon, W. Lin, J. C. Agar, C.-P. Wong, *Compos. Sci. Technol.* **2011**, *71*, 528.

[26] Z. Li, R. Zhang, K.-S. Moon, Y. Liu, K. Hansen, T. Le, C. P. Wong, *Adv. Funct. Mater.* **2013**, *23*, 1459.

[27] A. Goyal, A. Kumar, P. K. Patra, S. Mahendra, S. Tabatabaei, P. J. J. Alvarez, G. John, P. M. Ajayan, *Macromol. Rapid Commun.* **2009**, *30*, 1116.

[28] Z. Li, K. Hansen, Y. Yao, Y. Ma, K.-s. Moon, C. P. Wong, *J. Mater. Chem. C* **2013**, *1*, 4368.

[29] C. Yang, Y.-T. Xie, M. M.-F. Yuen, B. Xu, B. Gao, X. Xiong, C. P. Wong, *Adv. Funct. Mater.* **2010**, *20*, 2580.

[30] a) R. Zhang, W. Lin, K.-s. Moon, C. P. Wong, *ACS Appl. Mater. Interfaces* **2010**, *2*, 2637; b) R. W. Zhang, K. S. Moon, W. Lin, C. P. Wong, *J. Mater. Chem.* **2010**, *20*, 2018.

[31] a) J. Kost, A. Foux, M. Narkis, *Polym. Eng. Sci.* **1994**, *34*, 1628; b) P. E. Wack, R. L. Anthony, E. Guth, *J. Appl. Phys.* **1947**, *18*, 456.

[32] a) M. H. G. Wichmann, S. T. Buschhorn, J. Gehrmann, K. Schulte, *Phys. Rev. B* **2009**, *80*; b) M. Park, H. Kim, J. P. Youngblood, *Nanotechnology* **2008**, 19.

[33] X. W. Zhang, Y. Pan, Q. Zheng, X. S. Yi, *J. Polym. Sci. Pol. Phys.* **2000**, *38*, 2739.

[34] a) K.-Y. Chun, Y. Oh, J. Rho, J.-H. Ahn, Y.-J. Kim, H. R. Choi, S. Baik, *Nat. Nano.* **2010**, *5*, 853; b) F. Xu, Y. Zhu, *Adv. Mater.* **2012**, *24*, 5117.

[35] R. Ma, S. Kwon, Q. Zheng, H. Y. Kwon, J. I. Kim, H. R. Choi, S. Baik, *Adv. Mater.* **2012**, *24*, 3344.

[36] M. Taya, W. J. Kim, K. Ono, *Mech. Mater.* **1998**, *28*, 53.

[37] C. Yang, M. Yuen, B. Gao, Y. Ma, C. Wong, *J. Electron. Mater.* **2011**, *40*, 78.

[38] X. Z. Niu, S. L. Peng, L. Y. Liu, W. J. Wen, P. Sheng, *Adv. Mater.* **2007**, *19*, 2682.

[39] Y. Kim, J. Zhu, B. Yeom, M. Di Prima, X. Su, J.-G. Kim, S. J. Yoo, C. Uher, N. A. Kotov, *Nature* **2013**, *500*, 59.

[40] L. Johansson, J. Enlund, S. Johansson, I. Katardjiev, V. Yantchev, *Biomedical. Microdevices* **2012**, *14*, 279.


© 2014 WILEY-VCH Verlag GmbH & Co. KGaA, Weinheim